Chinese Physics Letters **40**, 017401 (2023)

$Fe_{1+y}Te_xSe_{1-x}$: A Delicate and Tunable Majorana Material

Fazhi Yang(杨发枝)[1,2†], Giao Ngoc Phan[1,3†*], Renjie Zhang(张任杰)[1,2], Jin Zhao(赵金)[1,2], Jiajun Li(李佳俊)[1,2], Zouyouwei Lu(鲁邹有为)[1,2], John Schneeloch[4], Ruidan Zhong(钟瑞丹)[4,6], Mingwei Ma(马明伟)[1,5], Genda Gu(顾根大)[4], Xiaoli Dong(董晓莉)[1,2,5], Tian Qian(钱天)[1,5], and Hong Ding(丁洪)[1,3,6*]

[1]*Beijing National Laboratory for Condensed Matter Physics and Institute of Physics, Chinese Academy of Sciences, Beijing 100190, China*
[2]*School of Physics, University of Chinese Academy of Sciences, Beijing 100190, China*
[3]*CAS Center for Excellence in Topological Quantum Computation, University of Chinese Academy of Sciences, Beijing 100190, China*
[4]*Condensed Matter Physics and Materials Science Department, Brookhaven National Laboratory, Upton, NY, USA*
[5]*Songshan Lake Materials Laboratory, Dongguan 523808, China*
[6]*Tsung-Dao Lee Institute, Shanghai Jiao Tong University, Shanghai 201210, China*

(Received 30 October 2022; accepted manuscript online 12 December 2022)

We report the observation for the p_z electron band and the band inversion in $Fe_{1+y}Te_xSe_{1-x}$ with angle-resolved photoemission spectroscopy. Furthermore, we found that excess Fe ($y > 0$) inhibits the topological band inversion in $Fe_{1+y}Te_xSe_{1-x}$, which explains the absence of Majorana zero modes in previous reports for $Fe_{1+y}Te_xSe_{1-x}$ with excess Fe. Based on our analysis of different amounts of Te doping and excess Fe, we propose a delicate topological phase in this material. Thanks to this delicate phase, one may be able to tune the topological transition via applying lattice strain or carrier doping.

DOI: 10.1088/0256-307X/40/1/017401

Iron-based superconductors (FeSCs) become a promising platform for long-sought-after topological quantum computation, thanks to recent discoveries of topological surface states and Majorana zero modes (MZMs) in them.[1–7] The band inversion between the electron band of the chalcogen p_z orbital character and the hole band of the Fe d_{xz} character along the Γ–Z direction is crucial to realize the topological non-trivial surface states in FeSCs.[8,9] Fe(Te,Se) (or more precisely $Fe_{1+y}Te_xSe_{1-x}$) has the simplest structure among FeSCs. As doping Te into FeSe, the interlayer p–p coupling enhancement causes stronger k_z dispersion of the p_z band, bringing the p_z band close to the d_{xz} band. When the p_z and d_{xz} bands cross each other along the Γ–Z direction, the topological band inversion occurs, and a spin-orbital coupling (SOC) gap is opened between those bands. However, direct experimental evidence of the p_z band and the band inversion in Fe(Te,Se) is still a missing puzzle piece.[10,11] In Fe(Te,Se), the MZMs were observed only in a portion of the vortices induced by the external magnetic field[2,12] or even completely absent in the samples with excess Fe.[13] The former may be caused by hybridization induced by the vortex lattice[14,15] and the chemical potential fluctuations due to the strong inhomogeneity in Fe(Te,Se).[16–18] However, the absence of MZMs at the vortices in the excess-Fe samples $Fe_{1+y}Te_xSe_{1-x}$ has been a long-lasting puzzle.

In this Letter, we present a direct observation of the electron p_z band in Fe(Te,Se) and the excess-Fe effect on the band inversion in $Fe_{1+y}Te_{0.7}Se_{0.3}$ with angle-resolved photoemission spectroscopy (ARPES). The direct observations of the p_z electron band and the band inversion confirm the MZM nature of scanning-tunneling-microscopy/spectroscopy (STM/S) results reported before. The observed excess-Fe effect in $Fe_{1+y}Te_{0.7}Se_{0.3}$ gives a key insight into the absence of MZMs at the vortices in the excess-Fe samples.[13] Our analyses strongly suggest the delicate topological property in $Fe_{1+y}Te_xSe_{1-x}$, offering a practical platform for studying tunable MZMs.

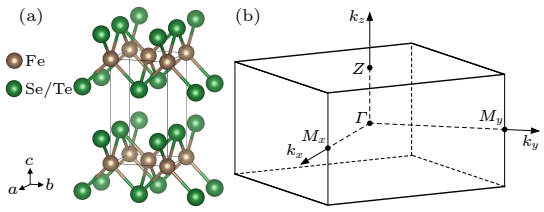

Fig. 1. (a) The crystal structure of Fe(Te,Se). (b) The corresponding Brillouin zone.

The crystal structure of Fe(Te,Se) is shown in Fig. 1(a). The excess Fe could exist at Fe(Te,Se) interlayers.[19] High-quality FeSe single crystals were grown by the chemical vapor transport method using a mixture of $AlCl_3$ and KCl as the transport agent.[20] High-quality $FeTe_{0.55}Se_{0.45}$ single crystals, free from excess Fe, were grown using the self-flux method. These samples originate from the same sample batch used in the previous STS report of the vortex MZMs.[2] High-quality $Fe_{1+y}Te_{0.7}Se_{0.3}$ single crystals were

†They contributed equally to this work.
*Corresponding authors. Email: dingh@sjtu.edu.cn; gphan@iphy.ac.cn
© 2023 Chinese Physical Society and IOP Publishing Ltd

grown by the unidirectional solidification method. With the method, an amount of excess Fe exists in as-grown samples $Fe_{1+y}Te_{0.7}Se_{0.3}$, and the excess Fe can be removed gradually via post-growth annealing in a sealed-vacuum-quartz tube to become $Fe_{1+k}Te_{0.7}Se_{0.3}$ ($k < y$). High-resolution ARPES measurements were carried out with an R4000 analyzer and a helium discharge lamp. The energy resolution is set at 5 meV, and the sample temperature is set at 30 K for all ARPES measurements.

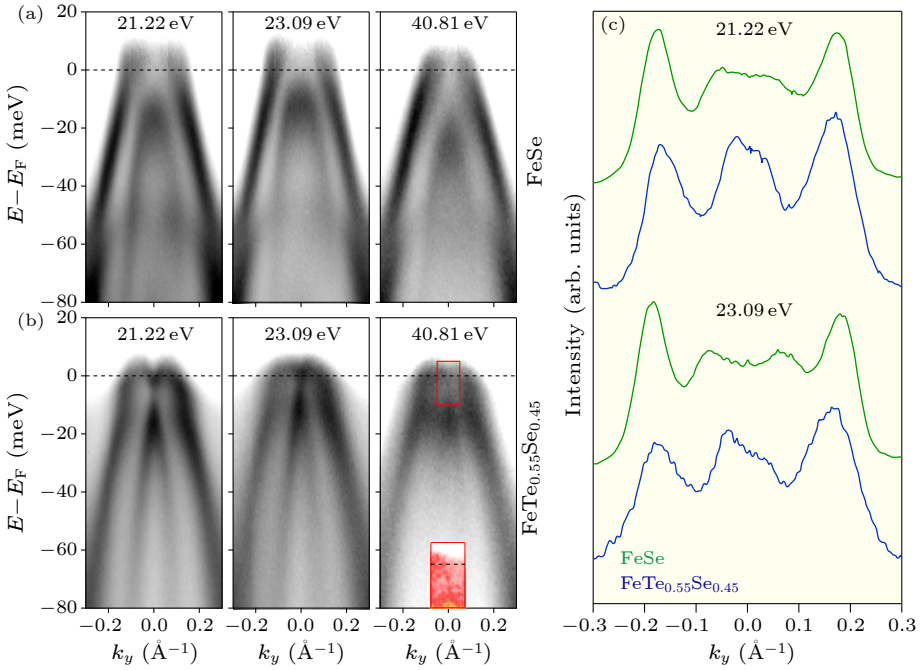

Fig. 2. (a) The ARPES intensities divided by the Fermi–Dirac distribution function at $T = 30$ K of FeSe measured along Γ–M with three different photon energies. The d_{xz} lower-hole-band intensity is weaker than that of the d_{yz} upper-hole-band due to the matrix element effect. These two hole-bands exhibit obvious k_z dispersion. (b) Similar to (a) but measured for $FeTe_{0.55}Se_{0.45}$. A shallow p_z electron band emerges above the Fermi level with strong k_z dispersion. (c) Comparison of the momentum distribution curves (MDCs) at the energy of 25 meV bellow the Fermi level for FeSe and $FeTe_{0.55}Se_{0.45}$ measured with different photon energies. The inner peaks correspond to the d_{xz} band, and the outer peaks correspond to the d_{yz} band. The intensity enhancement of the d_{xz} lower-hole-band top by factor of three indicates the band inversion between the p_z and d_{xz} bands. Inset: A weak linear-dispersion state can be resolved, thanks to the absence of the p_z band in its vicinity, which is similar to the Dirac-cone surface states observed with laser ARPES reported before. [1]

Figure 2(a) shows the ARPES intensities divided by the Fermi distribution function of FeSe. The ARPES intensities were measured along the Γ–M direction with three different photon energies of 21.22, 23.09, and 40.81 eV, corresponding to k_z of 4.53, 4.70, and $6.03\pi/c$, respectively. Two hole bands with clear k_z dispersion are observed along the Brillouin-zone center line Γ–Z.[21,22] The d_{xy} spectral intensity is too weak to be observed due to its large decoherence caused by strong orbital-selective correlations.[23] Benefited from the partially polarized light source, we can analyze the orbital character of these two hole bands using the matrix element effect. With the difference in the spectral intensity by a factor of three, the upper hole band with stronger spectral intensity and the lower band with weaker spectral intensity are mainly of d_{yz} and d_{xz} orbital characters, respectively. This orbital character is consistent with the experimental results reported for Fe(Te,Se).[22] In $FeTe_{0.55}Se_{0.45}$, similar to FeSe, a set of two-hole bands is also observed. Interestingly, we observed a shallow electron band emerging from above the Fermi level with the photon energies of 21.22 and 23.09 eV corresponding to k_z of $4.97\pi/c$ and $5.15\pi/c$, respectively, which are close to the Z point. At the same time, the electron band could not be observed with the photon energy of 40.81 eV corresponding to k_z of $6.61\pi/c$, which is between the Γ and Z points. The behavior of electron band is consistent with the p_z band predicted by theory and can be assigned to it.[8] Furthermore, the spectral intensity of the lower-hole-band top in $FeTe_{0.55}Se_{0.45}$ is enhanced by a factor of three to those in FeSe shown in the comparison of the momentum distribution curves (MDCs) in Fig. 2(c), indicating that the d_{xz} band may have undergone a band inversion with the p_z electron band. A linear-dispersion state can be resolved with the photon energy of 40.81 eV, thanks to the absence of the p_z band in its vicinity at k_z away from the Z point. The linear dispersion is similar to Dirac-cone surface states observed with laser ARPES reported before.[1] The emergence of the shallow electron band at the Fermi level in $FeTe_{0.55}Se_{0.45}$ with pronounced k_z dispersion confirms the previous theoretical prediction that Te doping brings the p_z band close to d_{xz}, promoting the topological band inversion and formation of the topological surface states.

To investigate the effect of Te doping and excess

Fe in $Fe_{1+y}Te_xSe_{1-x}$, we measured $Fe_{1+y}Te_{0.7}Se_{0.3}$ samples with different amounts of excess Fe. The ARPES intensity of the as-grown $Fe_{1+y}Te_{0.7}Se_{0.3}$ and annealed $Fe_{1+k}Te_{0.7}Se_{0.3}$ ($k < y$) are shown in Figs. 3(a) and 3(b), respectively. In contrast to the $FeTe_{0.55}Se_{0.45}$, the spectral intensity of the lower-hole-band top is much weaker or invisible with the photon energy of 40.81 eV. The weakening of intensity by a factor of 3 in d_{xz} band top intensity can be seen with the comparison of MDCs and energy distribution curves (EDCs) shown in Figs. 3(c) and 3(d), respectively. The strong and sharp peak of d_{xz} in $FeTe_{0.55}Se_{0.45}$ becomes weak and broader in the as-grown $Fe_{1+y}Te_{0.7}Se_{0.3}$ and annealed $Fe_{1+k}Te_{0.7}Se_{0.3}$. This suggests that the band inversion does not occur in $Fe_{1+y}Te_{0.7}Se_{0.3}$ samples with excess Fe. Therefore in $Fe_{1+y}Te_{0.7}Se_{0.3}$, both Te-doping and excess-Fe effects are involved simultaneously. To figure out the individual role of each effect on the band structure, we analyze the energy band positions for these observed spectra and plot the results as a function of k_z. The d_{xz} band top and the p_z band bottom are extracted from the EDCs by two Lorentzian fittings. Because the d_{yz} band top is in the unoccupied energy range, the d_{yz} top is determined via parabolic fitting of the d_{yz} band dispersions extracted from the momentum distribution curves (MDCs) by Lorentzian fitting.

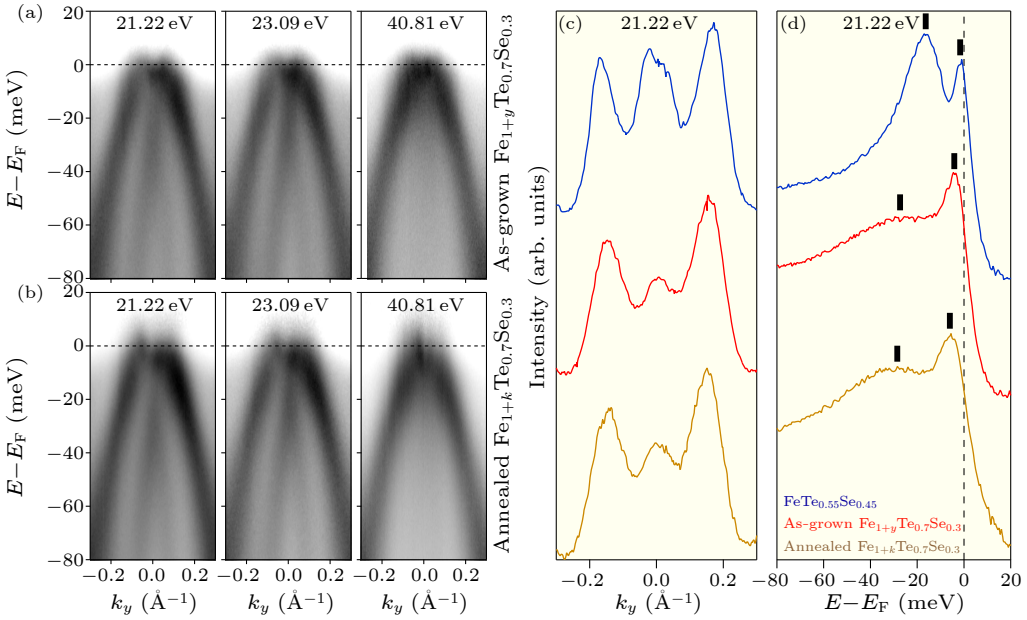

Fig. 3. (a) ARPES intensities of as-grown $Fe_{1+y}Te_{0.7}Se_{0.3}$ with different photon energies. (b) Same as (a) but for annealed $Fe_{1+k}Te_{0.7}Se_{0.3}$ ($k < y$). (c) Comparison of MDCs at the energy of 25 meV bellow the Fermi level for $FeTe_{0.55}Se_{0.45}$ in Fig. 2(b), as-grown $Fe_{1+y}Te_{0.7}Se_{0.3}$, and annealed $Fe_{1+k}Te_{0.7}Se_{0.3}$ measured with photon energy of 21.22 eV. The inner peaks correspond to the d_{xz} band, and the outer peaks correspond to the d_{yz} band. (d) Similar to (c) but for the energy distribution curves (EDCs) at $k_y = 0$. The bars indicate the peaks extracted from Lorentzian fitting. In contrast to $FeTe_{0.55}Se_{0.45}$, no intensity enhancement of the lower hole-band top implies that there is no band inversion in $Fe_{1+y}Te_{0.7}Se_{0.3}$ and $Fe_{1+k}Te_{0.7}Se_{0.3}$. The p_z band bottom shifts downward in the annealed $Fe_{1+k}Te_{0.7}Se_{0.3}$ compared to the as-grown $Fe_{1+y}Te_{0.7}Se_{0.3}$.

Since the c-axis increases monotonously to the Te doping level (x) shown in Fig. 4(f), the same photon energy probes at different k_z values for each doping level. Therefore, we present our analysis of band positions as a function of the relative k_z, which is the relative distance to its nearest Γ point. The energy positions of the p_z band bottom, and the d_{yz}, d_{xz} band tops are plotted as a function of the relative k_z shown in Figs. 4(a)–4(c). ΔE is defined as the energy gap between the p_z band bottom and the d_{xz} band top, as shown in Fig. 4(d). Increasing the Te doping level, the d_{yz} and d_{xz} bands seem less dispersive, which can be expected from the c-axis expansion Fig. 4(f).[24] Generally speaking, the c-axis expansion weakens the k_z dispersion in the band structure. In the vicinity of the Z point, the d_{xz} and d_{yz} bands shift downward with the in-plane-lattice expansion with increasing Te doping level shown in Fig. 4(f), in agreement with the in-plane-lattice-strain effect reported before.[25] A similar behavior is also observed for the p_z electron band. From FeSe to $FeTe_{0.55}Se_{0.45}$, the p_z band shifts downward from about 20 meV above the Fermi level[26] to the Fermi level vicinity at k_z around the Z point, and the p_z band slightly shifts downward more with increasing Te doping level to $Fe_{1+y}Te_{0.7}Se_{0.3}$. It is noteworthy that the energy position change of the d_{xz} band is more than twice the change of the p_z band around the Z point from $FeTe_{0.55}Se_{0.45}$ to $Fe_{1+y}Te_{0.7}Se_{0.3}$, enlarging ΔE in $Fe_{1+y}Te_{0.7}Se_{0.3}$. The increase in ΔE obstructs the topological band inversion between p_z and d_{xz} bands.

Furthermore, reduction of excess Fe shows negligible effects on the d_{yz} and d_{xz} hole bands but a visible effect on the p_z electron band. The p_z band shifts downward, resulting in a smaller ΔE, which is only 5 meV larger than that in $FeTe_{0.55}Se_{0.45}$. However, no band inversion could be observed for the $Fe_{1+k}Te_{0.7}Se_{0.3}$. In other words, ex-

cess Fe causes the p_z band shifts upward away from the d_{xz} band, obstructing the topological band inversion. For promoting the topological band inversion, annealing for a long time can altogether remove excess Fe in $x = 0.7$, bringing the p_z band close to the d_{xz} band. That is probably why Johnson *et al.* observed the topological band inversion in $FeTe_{0.7}Se_{0.3}$ with laser ARPES.[27,28] Surprisingly, the difference of 5 meV in the ΔE between $FeTe_{0.55}Se_{0.45}$ and $Fe_{1+k}Te_{0.7}Se_{0.3}$ causes a topological phase transition from the topological phase to the non-topological phase. Because of the sensitivity to ΔE, we propose the delicate topological phase in $Fe_{1+y}Te_xSe_{1-x}$.

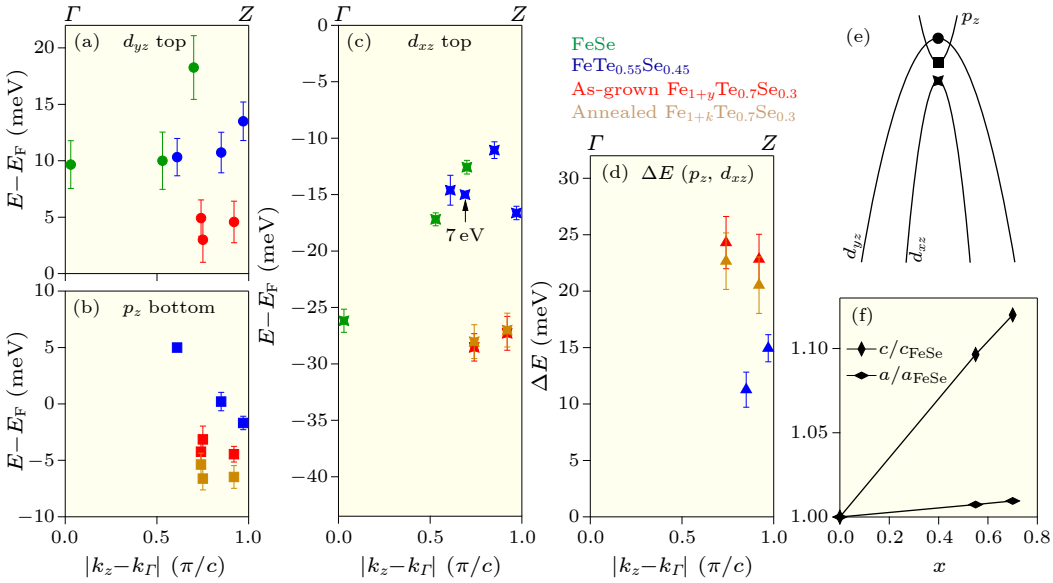

Fig. 4. (a)–(c) The energy positions of the d_{yz} band top, the p_z band bottom, and the d_{xz} band top [illustrated in (e)] plotted as a function of the relative k_z distance to its nearest Γ point. (d) The energy gap ΔE between the p_z band bottom and the d_{xz} band top plotted as a function of the relative k_z. (e) Schematic of the band structure in Fe(Te,Se). (f) The ratio of lattice parameters between different Te doping levels (x) and FeSe.[24]

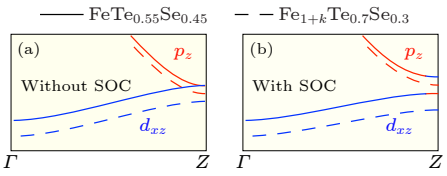

Fig. 5. Schematic of the band structures of different Te doping levels. $FeTe_{0.55}Se_{0.45}$ and $Fe_{1+k}Te_{0.7}Se_{0.3}$ are represented by solid and dashed lines, respectively. The d_{xz} and p_z orbital bands are labeled by red and blue colors. (a) Schematic of band structures without SOC. (b) Schematic of band structures with SOC.

Figure 5 illustrates the delicate topological phase in Fe(Te,Se). For $FeTe_{0.55}Se_{0.45}$, shown by the solid lines, the p_z band touches with the d_{xz} band around the Z point when SOC is not considered [Fig. 5(a)]. When SOC is considered, it opens a SOC gap of about 10 meV between the p_z and d_{xz} bands since there is no rotation symmetry protection, forming the band inversion [Fig. 5(b)].[8] Without SOC, as the p_z and d_{xz} bands just touch together in the topological phase, any effect that opens a crystal band gap between p_z and d_{xz} would lift the touching. Thus, in $Fe_{1+k}Te_{0.7}Se_{0.3}$ shown by dashed lines, without SOC, the excess Fe opens a crystal band gap between p_z and d_{xz} bands along the Γ–Z direction due to a greater downward shift of the d_{xz} band in comparison with that of the p_z band as shown in Fig. 5(a). When SOC is considered, the crystal band gap combines with the SOC gap, forming a larger ΔE than that in $FeTe_{0.55}Se_{0.45}$ as shown in Fig. 5(b). This larger ΔE in $Fe_{1+k}Te_{0.7}Se_{0.3}$ is consistent with our observation. Due to the delicate topological phase, besides the Te doping, the excess Fe is also a key parameter to control topological phase in $Fe_{1+y}Te_xSe_{1-x}$. The observed excess-Fe effect and the delicate topological phase can explain the absence of MZMs in some vortices in $FeTe_{0.55}Se_{0.45}$ or almost all vortices in the excess-Fe samples.[2,12,13] Interestingly, the delicate topological phase in $Fe_{1+y}Te_xSe_{1-x}$ makes itself a candidate for a tunable MZM platform as its ΔE can be practically manipulated using other parameters such as lattice strain or carrier doping.

In summary, we have observed direct experimental evidence of the p_z electron band and the topological band inversion in $Fe_{1+y}Te_xSe_{1-x}$. Our analysis results show that the excess Fe is a crucial parameter for controlling the topological phase in $Fe_{1+y}Te_xSe_{1-x}$, which makes it a candidate for tunable MZM platform by fine-tuning its delicate topological phase.

We thank Zhijun Wang, Lingyuan Kong, and Wenyao Liu for helpful discussions. This work was performed at Beijing National Laboratory for Condensed Matter Physics and Institute of Physics, Chinese Academy of Sciences, Beijing, China. This work was supported by the National Natural Science Foundation of China (Grant Nos. 11888101 and U1832202), the Chinese Academy of Sciences (Grant Nos. QYZDB-SSW-SLH043, XDB28000000, and XDB33000000), the K. C. Wong Education Foundation (Grant No. GJTD-2018-01), and the In-

formatization Plan of Chinese Academy of Sciences (Grant No. CAS-WX2021SF-0102). This work was also supported by the Synergetic Extreme Condition User Facility (SECUF). G.D.G. was supported by US DOE (Grant Nos. DE-SC0010526 and DE-SC0012704).

References

[1] Zhang P, Yaji K, Hashimoto T, Ota Y, Kondo T, Okazaki K, Wang Z J, Wen J S, Gu G D, Ding H, and Shik S 2018 *Science* **360** 182

[2] Wang D F, Kong L Y, Fan P, Chen H, Zhu S Y, Liu W Y, Cao L, Sun Y J, Du S X, Schneeloch J, Zhong R D, Gu G D, Fu L, Ding H, and Gao H J 2018 *Science* **362** 333

[3] Liu W Y, Cao L, Zhu S Y, Kong L Y, Wang G W, Papaj M, Zhang P, Liu Y B, Chen H, Li G, Yang F Z, Kondo T, Du S X, Cao G H, Shin S, Fu L, Yin Z P, Gao H J, and Ding H 2020 *Nat. Commun.* **11** 5688

[4] Fan P, Yang F Z, Qian G J, Chen H, Zhang Y Y, Li G, Huang Z H, Xing Y Q, Kong L Y, Liu W Y, Jiang K, Shen C M, Du S X, Schneeloch J, Zhong R D, Gu G D, Wang Z Q, Ding H, and Gao H J 2021 *Nat. Commun.* **12** 1348

[5] Kong L Y, Cao L, Zhu S Y, Papaj M, Dai G Y, Li G, Fan P, Liu W Y, Yang F Z, Wang X C, Du S X, Jin C Q, Fu L, Gao H J, and Ding H 2021 *Nat. Commun.* **12** 4146

[6] Li M, Li G, Cao L, Zhou X T, Wang X C, Jin C Q, Chiu C K, Pennycook J S, Wang Z Q, and Gao H J 2022 *Nature* **606** 890

[7] Liu W Y, Hu Q X, Wang X C, Zhong Y G, Yang F Z, Kong L Y, Cao L, Li G, Okazaki K, Kondo T, Jin C Q, Zhang F C, Xu J P, Gao H J, and Ding H 2022 *Quantum Front* **1** 20

[8] Wang Z J, Zhang P, Xu G, Zeng L K, Miao H, Xu X Y, Qian T, Weng H M, Richard P, Fedorov A V, Ding H, Dai X, and Fang Z 2015 *Phys. Rev. B* **92** 115119

[9] Zhang P, Wang Z J, Wu X X *et al.* 2019 *Nat. Phys.* **15** 41

[10] Lohani H, Hazra T, Ribak A, Nitzav Y, Fu H X, Yan B H, Randeria M, and Kanigel A 2020 *Phys. Rev. B* **101** 245146

[11] Peng X L, Li Y, Wu X X, Deng H B, Shi X, Fan W H, Li M, Huang Y B, Qian T, Richard P, Hu J P, Pan S H, Mao H Q, Sun Y J, and Ding H 2019 *Phys. Rev. B* **100** 155134

[12] Machida T, Sun Y, Pyon S, Takeda S, Kohsaka Y, Hanaguri T, Sasagawa T, and Tamegai T 2019 *Nat. Mater.* **18** 811

[13] Chen M Y, Chen X Y, Yang H, Du Z Y, Zhu X Y, Wang E Y, and Wen H H 2018 *Nat. Commun.* **9** 970

[14] Chiu C K, Machida T, Huang Y Y, Hanaguri T, and Zhang F C 2020 *Sci. Adv.* **6** eaay0443

[15] Pathak V, Plugge S, and Franz M 2021 *Ann. Phys.* **435** 168431

[16] Kong L Y, Zhu S Y, Papaj M, Chen H, Cao L, Isobe H, Xing Y Q, Liu W Y, Wang D F, Fan P, Sun Y J, Du S X, Schneeloch J, Zhong R D, Gu G D, Fu L, Gao H J, and Ding H 2019 *Nat. Phys.* **15** 1181

[17] Li Y M, Zaki N, Garlea V O, Savici A T, Fobes D, Xu Z J, Camino F, Petrovic C, Gu G D, Johnson P D, Tranquada J M, and Zaliznyak I A 2021 *Nat. Mater.* **20** 1221

[18] Singh U R, White S C, Schmaus S, Tsurkan V, Loidl A, Deisenhofer J, and Wahl P 2013 *Phys. Rev. B* **88** 155124

[19] Yin J X, Wu Z, Wang J H, Ye Z Y, Gong J, Hou X Y, Shan L, Li A, Liang X J, Wu X X, Li J, Ting C S, Wang Z Q, Hu J P, Hor P H, Ding H, and Pan S H 2015 *Nat. Phys.* **11** 543

[20] Li H, Ma M W, Liu S B, Zhou F, and Dong X L 2020 *Chin. Phys. B* **29** 127404

[21] Nakayama K, Miyata Y, Phan G N, Sato T, Tanabe Y, Urata T, Tanigaki K, and Takahashi T 2014 *Phys. Rev. Lett.* **113** 237001

[22] Zhang P, Qian T, Richard P, Wang X P, Miao H, Lv B Q, Fu B B, Wolf T, Meingast C, Wu X X, Wang Z Q, Hu J P, and Ding H 2015 *Phys. Rev. B* **91** 214503

[23] Yin Z P, Haule K, and Kotliar G 2011 *Nat. Mater.* **10** 932

[24] Sales B C, Sefat A S, McGuire M A, Jin R Y, Mandrus D, and Mozharivskyj Y 2009 *Phys. Rev. B* **79** 094521

[25] Phan G N, Nakayama K, Sugawara K, Sato T, Urata T, Tanabe Y, Tanigaki K, Nabeshima F, Imai Y, Maeda A, and Takahashi T 2017 *Phys. Rev. B* **95** 224507

[26] Kasahara S, Watashige T, Hanaguri T, Kohsaka Y, Yamashita T, Shimoyama Y, Mizukami Y, Endo R, Ikeda H, Aoyama K, Terashima T, Uji S, Wolf T, Lohneysen H, Shibauchi T, and Matsuda Y 2014 *Proc. Natl. Acad. Sci. USA* **111** 16309

[27] Zaki N, Gu G D, Tsvelik A, Wu C J, and Johnson P D 2021 *Proc. Natl. Acad. Sci. USA* **118** e2007241118

[28] Rameau J D, Zaki N, Gu G D, Johnson P D, and Weinert M 2019 *Phys. Rev. B* **99** 205117